ELSEVIER

Polymer 40 (1999) 2745–2757

polymer

Isotactic polypropylene/ethylene-co-propylene blends: effects of the copolymer microstructure and content on rheology, morphology and properties of injection moulded samples

L. D'Orazio[a,*], C. Mancarella[a], E. Martuscelli[a], G. Cecchin[b], R. Corrieri[b]

[a]*Istituto di Ricerca e Tecnologia delle Materie Plastiche del CNR, Via Toiano, 6-80072 Arco Felice, Naples, Italy*
[b]*Montell Italia S.p.A, Ferrara, Italy*

Received 23 April 1997; revised 19 May 1998; accepted 16 June 1998

Abstract

Melt rheology, phase morphology and properties of (60/40) isotactic polypropylene/ethylene-co-propylene (iPP/EPR) blends containing EPR copolymer synthesized by means of a titanium based catalyst with very high stereospecific activity (EPR_{Ti}) were compared to that of (60/40) iPP/EPR blends containing EPR copolymer synthesized by using a traditional vanadium based catalyst (EPR_V). It was found that both the melts are to be classified 'negative deviation blends' and that for such a composition the copolymer represents the dispersed phase. SEM investigations showed in fact that the EPR phase segregate in to irregular shaped domains localized in the core of the bars, the dispersion coarseness increasing with an increase in the ratio between the EPR viscosity and iPP viscosity. At low temperatures the iPP impact strength was improved, comparatively better properties being shown by the blends containing the EPR_V copolymer. The different behaviour of EPR_{Ti} and EPR_V phases as impact modifiers was ascribed to their both different dispersion degree and microstructure. For test temperatures higher than EPR T_g the ethylenic crystallinity exhibited by the EPR_{Ti} phase was considered to induce toughening deterioration by decreasing tie molecules density in the EPR_{Ti} domains, notwithstanding the beneficial effect of the ethylenic build-up. The reduction in iPP crystallinity index (X_c) value found for iPP/EPR_{Ti} blends indicated a strong interference of the crystallization process of EPR_{Ti} ethylenic sequences with the iPP crystallization process. SAXS investigations revealed in addition that the iPP/EPR_{Ti} materials are characterized by an amorphous interlamellar layer (L_a) higher than that shown by plain iPP and iPP phase crystallized in presence of EPR_V copolymer. Taking also into account results obtained studying blends containing lower content of such EPR phases composition effects were investigated. WAXS studies showed that with increasing copolymer content the ratio between the apparent crystal size of iPP phase grown in a direction perpendicular to the (110) crystallographic plane [$D_{(110)}$] and that grown in direction perpendicular to the (040) crystallographic plane [$D_{(040)}$] increases. Such an effect was related to an increased iPP nucleation density according to DSC results.

Keywords: Polypropylene; Ethylene–propylene copolymers; Blends

1. Introduction

The role played by the molecular parameters of the components on melt rheology, phase morphology and toughening of blends of isotactic polypropylene (iPP) and ethylene-co-propylene copolymers (EPR), with the focus on 80/20 composition, were treated in detail [1–5]. It was shown that the desired final properties can be imparted by an appropriate choice of molecular mass and molecular mass distribution, constitution and tacticity of the blend components. A further critical factor is represented by the iPP crystallization conditions through which it is possible to optimize the overall phase structure.

With the aim at deepening the effects of the EPR microstructure (particularly effects of distribution of composition and sequences length of the structural units) on the structure-properties correlations so far established for iPP/EPR pairs, in the present paper we report on results of studies dealing with blends containing EPR copolymer synthesized by means of a Titanium based catalyst with very high stereospecific activity (EPR_{Ti}) and with blends containing EPR copolymer synthesized by using a traditional vanadium based catalyst (EPR_V). The EPR samples were synthesized 'ad hoc' to exhibit comparable propylene content, average molecular masses and molecular mass distribution. Melt rheology, phase morphology and properties of 60/40 materials have therefore been investigated and compared.

Taking also into account results obtained studying melt

* Corresponding author.

0032-3861/99/$ - see front matter
PII: S0032-3861(98)00504-7

rheology, phase morphology and impact behaviour of 80/20 iPP/EPR_{Ti} and iPP/EPR_V blends [6] composition effects were also investigated.

2. Experimental

2.1. Materials

The materials used in this study were an isotactic polypropylene (iPP) (HS005) made by Himont and two ethylene-propylene copolymers (EPR) synthesized at the Himont–'Giulio Natta' Research Centre following two different procedures: the first was a synthesis process in gas phase with a titanium based catalytic system, the second one a suspension polymerization with vanadium based catalytic system. The EPR copolymers so obtained were referred to as EPR_{Ti} and EPR_V, respectively. The average molecular masses and molecular masses distribution of the starting polymers determined by means of gel permeation chromatography (GPC) in ortho-dichlorobenzene at the temperature of 135°C are reported in Table 1.

2.2. Blending and sample preparation

The iPP and EPR copolymers were mixed in a Werner mixer with a blending time of 3.5 min. Blends with composition 60/40 (wt/wt) were prepared. After blending the materials were injection moulded by means of an injection press at 260°C with a mould temperature of 60°C.

2.3. Techniques

2.3.1. Oscillatory shearing flow properties

The oscillatory shearing flow properties, namely the complex viscosity η^* (defined by $\eta^* = \eta' - i\eta''$, where η' is the dynamic viscosity or the real part of the viscosity and η'' is the imaginary part of the viscosity), the storage modulus G' (defined by $G' = \omega\eta''$, where ω is the frequency of the oscillations in radians per second) and the loss modulus G'' (defined by $G'' = \omega\eta'$) of the plain components and blends were determined at 200°C and 250°C by means of a rheometrics mechanical spectrometer in the plate–plate mode with a constant strain and an angular frequency ranging between 0.01 and 100 rad s^{-1}.

2.3.2. Differential scanning calorimetry

The thermal behaviour of the single components and blends was analyzed by means of a differential scanning calorimeter Mettler TA 3000 equipped with a control and programming unit (microprocessor Tc 10). The apparent melting temperatures (T'_m) and the crystallinity indices (X_c) of the single components and blends were determined following this procedure: the samples were heated from room temperature up to 200°C with a rate of 10°C min^{-1} and the heat evolved during the scanning process (dH/dt) was recorded as a function of temperature. The T'_m values and the apparent enthalpies of melting (ΔH^*) were obtained from the maxima and the area of the melting peaks, respectively. The crystallinity indices were calculated from the ratio between ΔH^* value and the enthalpy of melting of 100% crystalline phase (ΔH^o).

The effect of nucleating ability of EPR phase on crystallization process of iPP was investigated following this procedure: the samples were heated from room temperature up to 200°C with a rate of 10°C min^{-1} and kept at this temperature for 10 min and then they were cooled with a rate of 10°C min^{-1}.

2.3.3. Dynamic mechanical thermal analysis

The tangent δ and storage modulus of samples of single components and blends were measured by means of a dynamic mechanical thermal analysis (Rheometric Scientific MK III). Test data was collected in tensile mode from −100°C to 100°C using a scanning rate of 1.5°C min^{-1} and a frequency of 1 Hz.

2.3.4. Scanning electron microscopy

iPP/EPR cryogenical fracture surfaces of injection moulded samples after coating with gold-palladium were observed by means of a scanning electron microscope (Philips 501).

2.3.5. Wide angle X-ray scattering

Wide angle X-ray scattering (WAXS) studies were carried out on samples of single components and blends by means of a PW 1060/71 Philips diffractometer (Cu Kα Ni-filtered radiation) equipped with sample spinning, the high voltage was 40 kV and the tube current was 30 mA.

2.3.6. Small angle X-ray scattering

Small angle X-ray scattering (SAXS) studies were carried out on samples of single components and blends

Table 1
Number-average molecular mass ($\bar{M}_n$), weight-average molecular mass ($\bar{M}_w$), molecular mass distribution ($\bar{M}_w/\bar{M}_n$), glass transition temperature (T_g) and apparent melting temperature (T'_m) for plain iPP and EPR copolymers together with the EPR propylene content (C_3)

Sample	$\bar{M}_n \cdot 10^3$	$\bar{M}_n \cdot 10^3$	$\bar{M}_w/\bar{M}_n$	C_3 content (% wt/wt)	T_g (°C)	T'_m (°C)
iPP	78.7	509	6.5	—	7	165
EPR_{Ti}	34.8	213	6.1	38.5	−41	122[a]
EPR_V	30.8	199	6.5	38.5	−43	—

[a]Polyethylenic sequences.

by means of a compact Kratky camera equipped with a Braun one-dimensional positional sensitive detector. Ni-filtered Cu Kα radiation generated from a Philips X-ray generator (PW 1730/10) operating at 40 kV and 30 mA was used. The raw scattering data were corrected for parasitic scattering, absorption and slit smearing by using Vonk's method [7]. The desmeared intensities were then Lorentz factor corrected by multiplying by s^2 ($s = 2\sin\theta/\lambda$) [8].

2.3.7. Impact strength and elastic behaviour

Notched Izod impact strengths of injection moulded samples were measured by means of a Ceast pendulum in a temperature range from − 60°C to 23°C according to ASTM D256. The elastic modulus of the materials was determined by means of an Instron machine at room temperature according to ASTM D638.

3. Results and discussion

3.1. Melt rheology

3.1.1. Dynamic viscoelastic properties

Fig. 1 shows the dependence of the logarithm of the modulus value of the complex viscosity $|\eta^*|$ upon the logarithm of the investigated frequencies at the temperatures of 200°C and 250°C for $(60/40)_{Ti}$ and $(60/40)_V$ blends. As shown and as expected, such melts are pseudo-plastic, i.e. $|\eta^*|$ values decrease with increasing frequency. Moreover for a given frequency the observed decrease in systems viscosity depends on temperature. With increasing temperature both the melts exhibit a lower sensitivity to frequency (see Fig. 1) indicating that the entanglements concentration decreases with increasing temperature. At the temperature of 200°C $(60/40)_{Ti}$ and $(60/40)_V$ melts exhibit, for a given frequency,

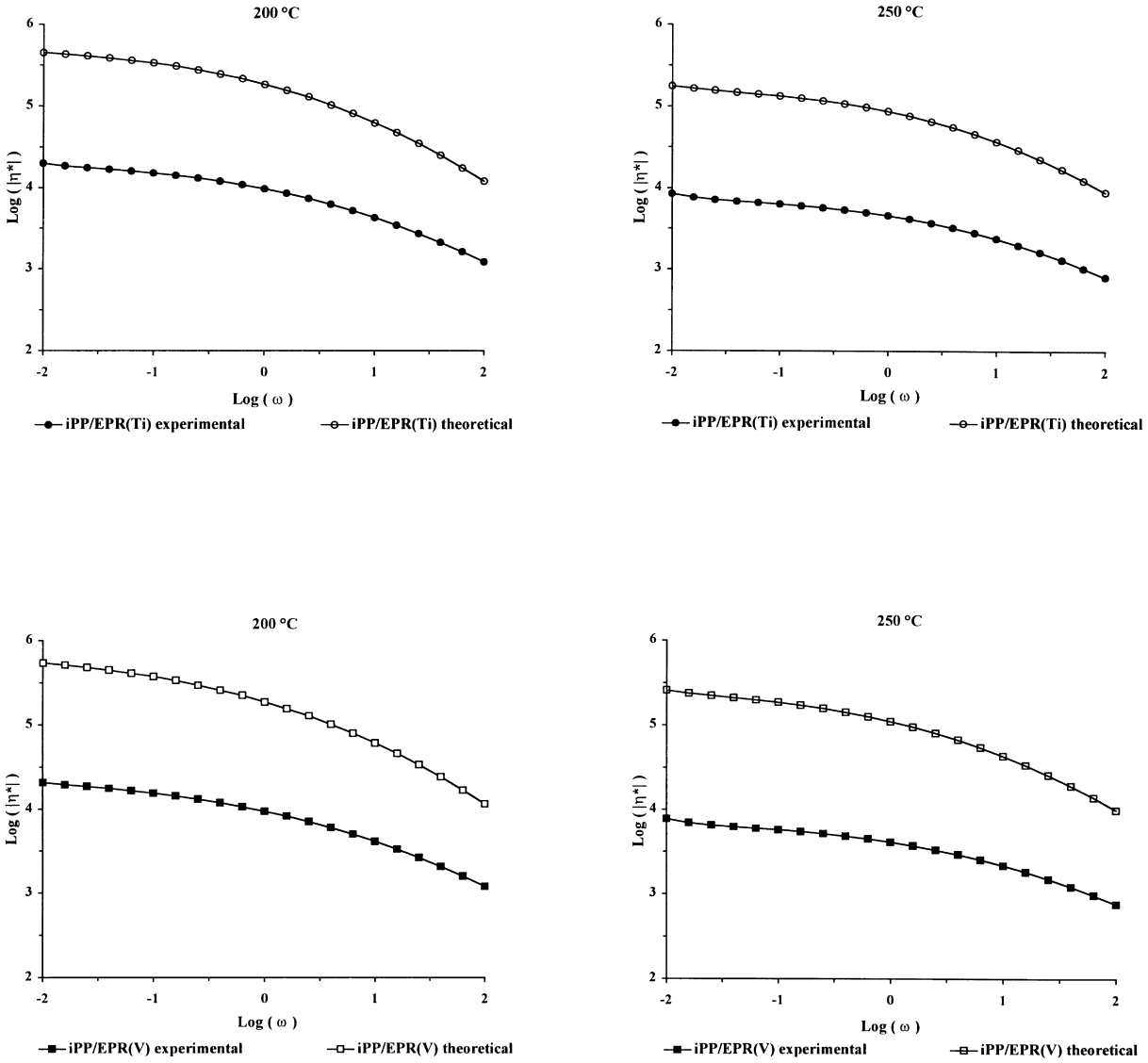

Fig. 1. Logarithm of the modulus value of the complex viscosity ($|\eta^*|$) as a function of the logarithm of the frequency (ω) for iPP/EPR blends at the temperatures of 200°C and 250°C.

comparable $|\eta^*|$ values, whereas with increasing temperature lower $|\eta^*|$ values are shown by the EPR_V containing system. Such results indicate that at 250°C the iPP/EPR_V melt is characterized by lower entanglements concentration and/or that the entanglements have time to slip and relax out the stresses.

As shown in Fig. 1 for both iPP/EPR systems mixing results in a decrease in viscosity below the mean value of the plain components, such a decrease becoming larger with decreasing frequency in agreement with results obtained studying 80/20 (wt/wt) blends [6]. This effect is designated as a 'negative deviation' from the following logarithm rule of mixture that applies at constant temperature and shear rate [9,10]:

$$\log\eta = \phi_1 \log\eta_1 + \phi_2 \log\eta_2$$

where η is the viscosity of the mixture, η_1 and η_2 are the viscosities of the two components measured at the same temperature and ϕ_1 and ϕ_2 are their volume fractions. Moreover for both iPP/EPR melts the extent of the observed negative deviation as a function of frequency increases with increasing test temperature (see Fig. 1). Such a finding is to be related to the lower sensitivity shown by the melts to frequency with increasing temperature.

Figs 2–5 show for $(60/40)_{Ti}$ and $(60/40)_V$ blends the dependence of the logarithm of G' and G'' values upon the

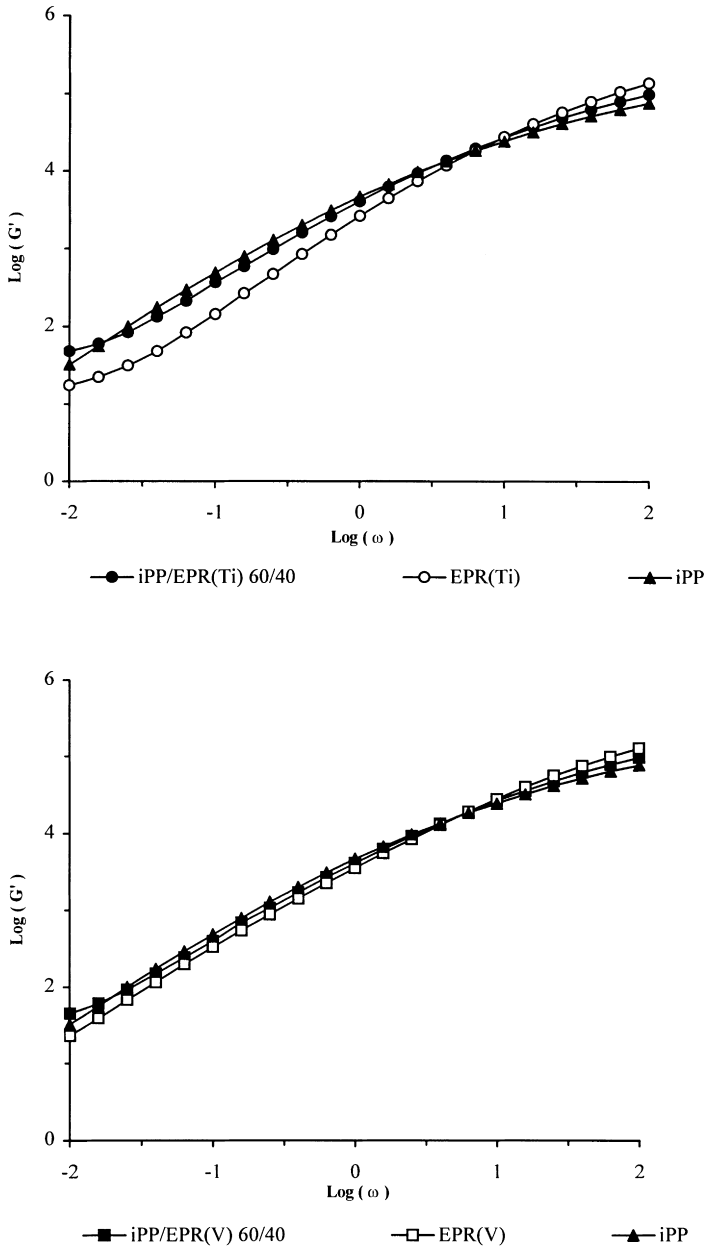

Fig. 2. Logarithm of the storage modulus G' as a function of the logarithm of the frequency (ω) for plain components and iPP/EPR blends at the temperature of 200°C.

logarithm of the investigated frequencies at the temperatures of 200°C and 250°C, in each plot the modulus logarithm of the single components is also reported. As shown by the comparison among such figures, the amounts of energy stored and dissipated by both the systems decreases on increasing temperature. For a given temperature the amounts of energy stored and dissipated seem to depend upon frequency rather than upon the EPR microstructure. In the first two decades the G' and G'' values shown by both the iPP/EPR systems result in fact higher or comparable to that exhibited by the plain iPP, whereas in the last frequency decade such values investigated range between those shown by the single components.

Note moreover that at the temperature of 200°C $(60/40)_{Ti}$ and $(60/40)_{V}$ melts show comparable G' and G'' values as a function of frequency. With increasing temperature, for a given frequency, comparatively larger amounts of energy are stored and dissipated by the iPP/EPR_{Ti} melt, the extent of the observed increase being larger for G' values. Such findings suggest that with increasing temperature the iPP/EPR_{Ti} melt is characterized by a higher entanglements concentration and/or by higher time to relax out the stress.

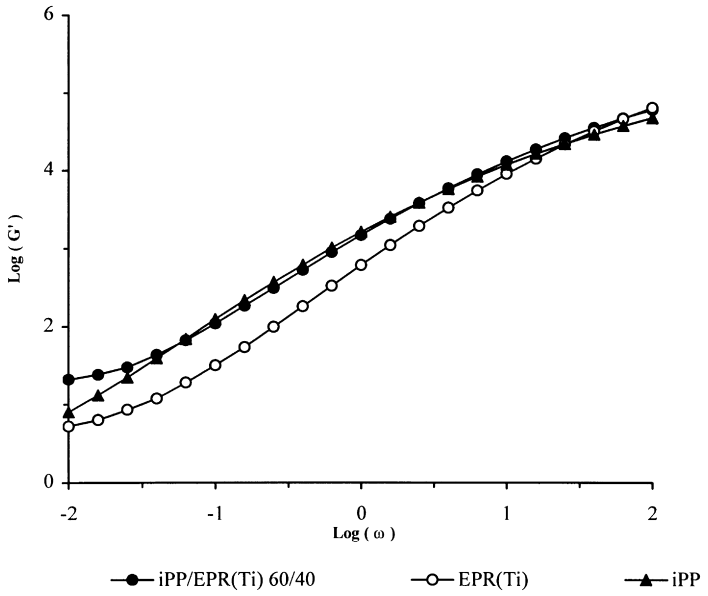

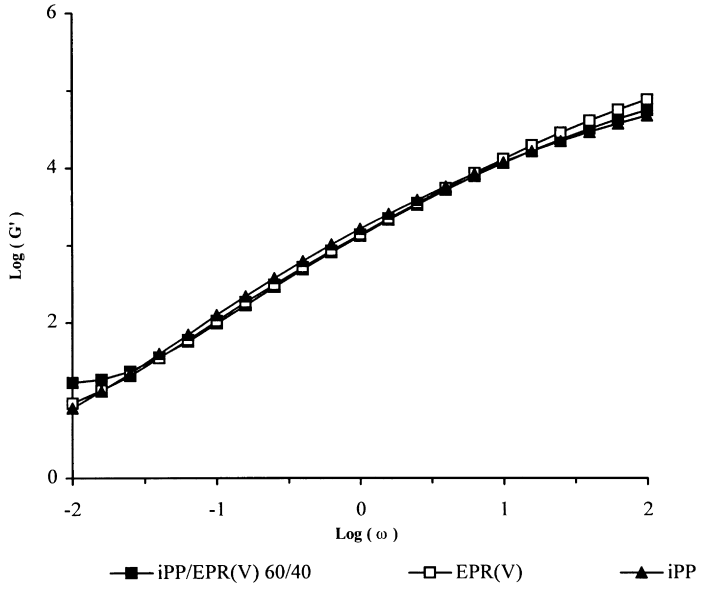

Fig. 3. Logarithm of the storage modulus G' as a function of the logarithm of the frequency (ω) for plain components and iPP/EPR blends at the temperature of 250°C.

3.1.2. Determination of zero-shear viscosity and activation energy for viscous flow

Taking into account that in oscillatory measurements on polymer melts the frequency (ω) becomes analogous to shear rate ($\dot{\gamma}$) [11–14] and assuming an approximate equivalence of η^* and apparent viscosity (η_a) [14–19], the zero-shear viscosity (η_0) of both single components and blends was calculated by using the following modified Cross–Bueche equation [20]:

$$\frac{\eta_0}{\eta_a} = 1 + (\alpha\dot{\gamma})^m$$

where η_0 is the zero-shear viscosity, α is a parameter that according to Cross should correspond to the characteristic relaxation time related to molecular mass for the linear polymer solution and m gives a measure of the shear-thinning of the melt, i.e. a measure of decrease in viscosity with increasing rate of shear. According to Iwakura et al. [21] for polymer melts α is related to the size of the apparent flow unit, the reciprocal of α corresponds to the shear rate at which $\eta_a = \eta_0/2$. From the lines $1/\eta_a$ versus $\dot{\gamma}^m$ the zero shear viscosity η_0 and α values are easily obtained from the reciprocal of the intercept and from slope respectively.

The m, η_0 and α values of the single components and blends at the temperatures of 200°C and 250°C are reported in Table 2 and Table 3, respectively, for the blends the zero

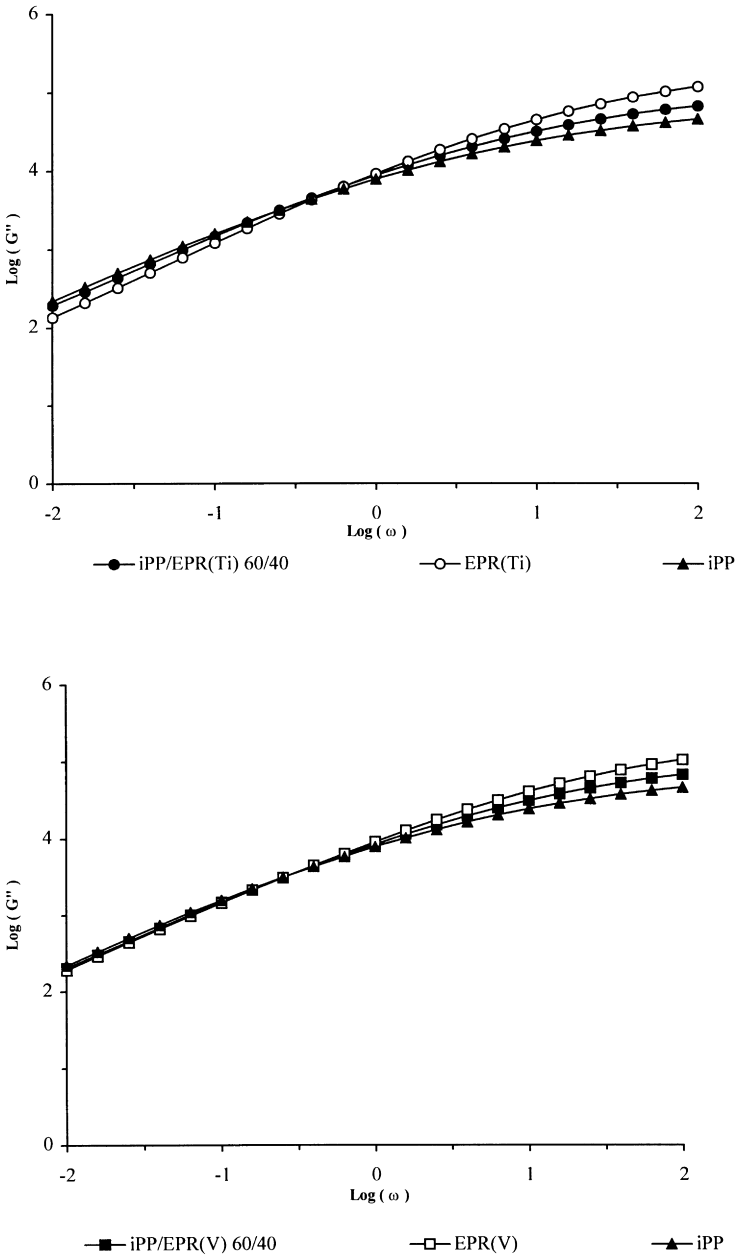

Fig. 4. Logarithm of the loss modulus G'' as a function of the logarithm of the frequency (ω) for plain components and iPP/EPR blends at the temperature of 200°C.

Table 2
Application of Cross equation: values of η_0, α and m for plain iPP and EPR copolymers at the temperatures of 200°C and 250°C

Sample	η_0 (Pa)		α (s)		m	
	200°C	250°C	200°C	250°C	200°C	250°C
iPP	18791	8200	0.886	0.804	2/3	4/7
EPR_{Ti}	12489	4271	0.138	0.078	2/3	4/7
EPR_V	17383	7298	0.488	0.233	4/7	6/11

shear viscosity values calculated assuming the additivity logarithm rule (η_0') are also reported. The application of the Cross equation to iPP/EPR blends reveals that, for a given temperature, slightly higher η_0 and α values are obtained for the blend containing the EPR_{Ti} copolymer, the same value being found for the m parameter (2/3) (see Table 3). Moreover the η_0 values of both the blends show a negative deviation from the logarithm additivity rule, the extent of such a deviation decreasing strongly on increasing the temperature (see η_0' values in Table 3).

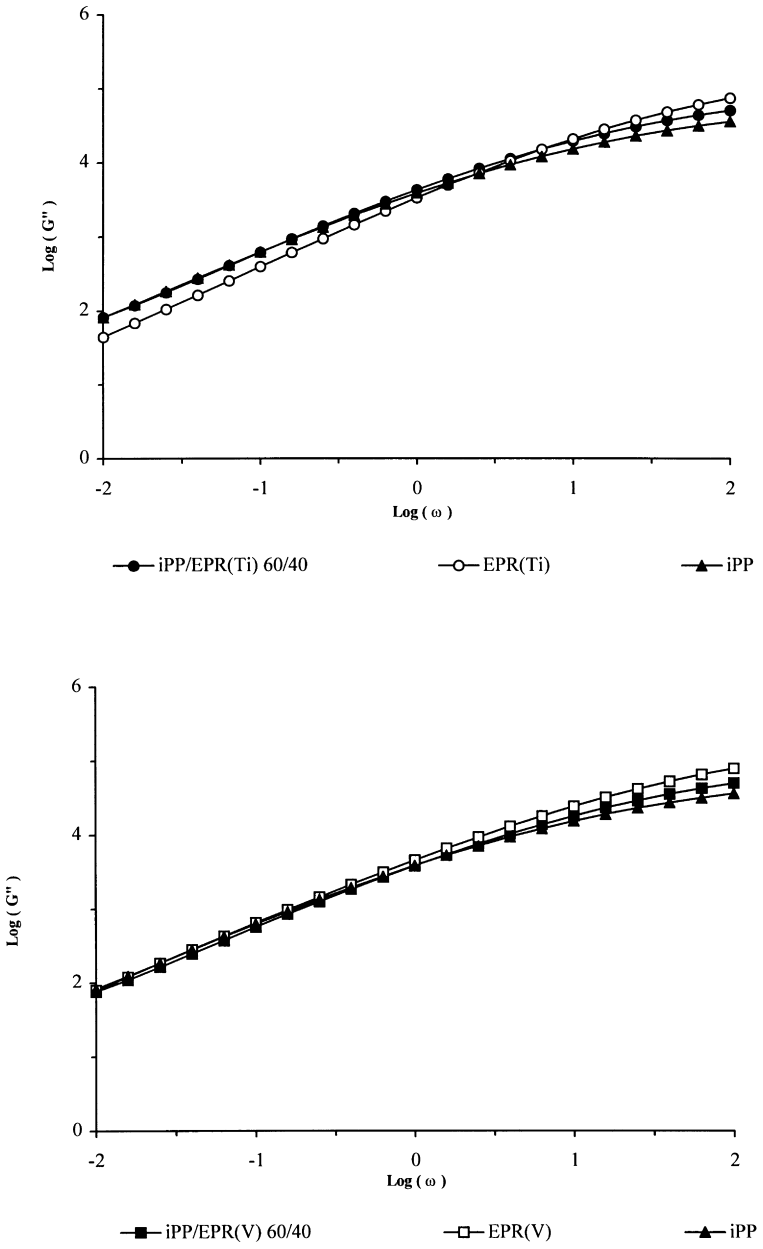

Fig. 5. Logarithm of the loss modulus G'' as a function of the logarithm of the frequency (ω) for plain components and iPP/EPR blends at the temperature of 250°C.

Table 3
Application of Cross equation: values of η_0, α and m for iPP/EPR blends together with the zero-shear viscosity values calculated assuming log additivity (η_0') and the melt flow viscosity ratio (μ) at the temperatures of 200°C and 250°C

Sample	η_0 (Pa)		α (s)		m		η_0' (Pa)		μ	
	200°C	250°C	200°C	250°C	200°C	250°C	200°C	250°C	200°C	250°C
$(60/40)_{Ti}$	16040	7527	0.427	0.397	2/3	4/7	375562	172109	0.66	0.57
$(60/40)_V$	15905	6623	0.381	0.351	2/3	4/7	451129	243630	0.92	0.89

The activation energy for the viscous flow values (ΔE^*) for the single components and blends, obtained by applying the following exponential relation accounting for the temperature dependence of the viscosity at temperatures far above the T_g or the melting point [22]:

$$\eta_0 = A\exp(\Delta E^*/RT)$$

where A is a constant characteristic of the polymer and its molecular mass, ΔE^* is the activation energy for the viscous flow (Table 4, R is the gas constant and T is the temperature in Kelvin degrees, for comparison the ΔE^* values obtained for the blends containing the 20% (wt/wt) are also reported. As shown the $(60/40)_V$ melt exhibits a ΔE^* value noticeably higher than that shown by the $(60/40)_{Ti}$ melt, thus indicating a higher volume of the flow element. The ΔE^* value found for the $(60/40)_{Ti}$ system closely approaches that shown by the plain iPP. Note moreover that the ΔE^* values of such iPP/EPR pairs are composition dependent, i.e. such values increase with increasing copolymer content (wt/wt) (see Table 4).

3.2. Thermal behaviour and crystallinity

DMTA analysis shows that both $(60/40)_{Ti}$ and $(60/40)_V$ systems exhibit, as expected, two distinct glass transition temperatures (T_g) to be ascribed to EPR and iPP components, respectively. Such T_g values are reported in Table 5 and are comparable to that found for blends containing lower EPR amounts (20% wt/wt) [1–6]. The DSC thermograms of samples of the $(60/40)_V$ blends show a single endothermic peak whose temperature position is characteristic of the melting of the α-form of iPP (see Table 5). Two endothermic peaks are shown by samples of the $(60/40)_{Ti}$ blends, the temperature positions of such peaks are characteristic of the melting of linear polyethylene (PE) and α-form of iPP, respectively (see Table 5). All the above results indicate that the immiscibility between iPP and EPR, both in the amorphous condensed and in the melted state, are independent of composition.

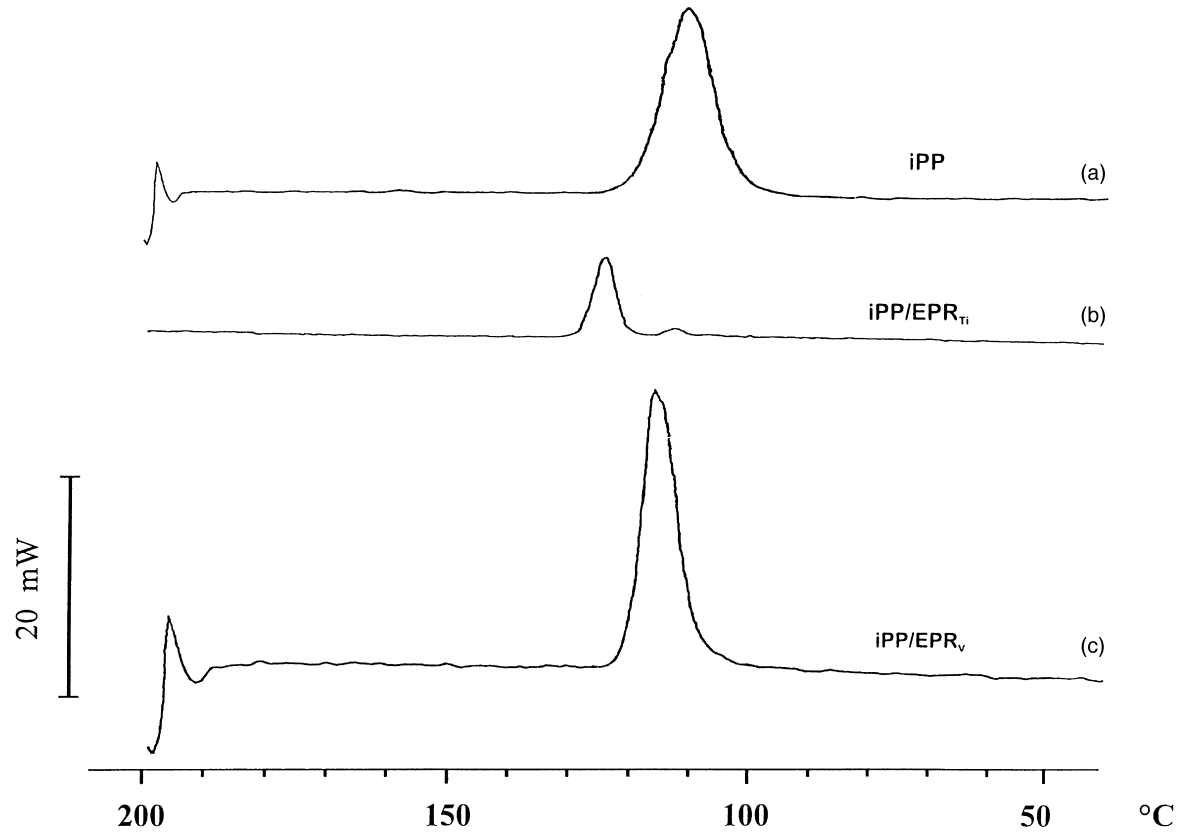

Fig. 6. Non-isothermal crystallization curve of: (a)the plain iPP; (b) iPP/EPR$_{Ti}$; and (c) iPP/EPR$_V$.

Table 4
Activation energy for the viscous flow (ΔE^*) for plain iPP and for iPP/EPR blends

Sample	ΔE^* (J mol^{-1})
iPP	14823
$(60/40)_{Ti}$	13525
$(60/40)_{V}$	21106
$(80/20)_{Ti}$	11548
$(80/20)_{V}$	14888

On the other hand it is interesting to observe that the crystallinity index (X_c) of iPP phase crystallized in the presence of EPR_{Ti} copolymer results depressed noticeably (see Table 5) suggesting an interference of the crystallization process of the EPR_{Ti} ethylenic sequences with the crystallization process of the iPP phase. From previous study [6] it was shown that the chain of the EPR_{Ti} copolymer is characterized by the presence of long ethylenic sequences with constitutional and configurational regularity required for crystallization of PE phase occurring. Taking into account that the iPP phase crystallized from its blends containing the 20% (wt/wt) of EPR_{Ti} copolymer showed X_c values comparable to that exhibited by the plain iPP [6], the result suggests that the iPP crystallization process in presence of EPR_{Ti} phase can be strongly affected by composition.

The non-isothermal crystallization exotherms of the plain iPP and of iPP/EPR blends are shown in Fig. 6, the crystallization exotherm of the EPR_{Ti} ethylenic sequences showed that such sequences crystallize between 111°C and 88°C (see Table 5), the temperature position of the maximum of the peak being at 102°C. As shown in Fig. 6 when the iPP crystallizes in the presence of EPR_{Ti} or EPR_{V} phase the crystallization peak shifts to higher temperatures indicating that both the copolymers contain heterogeneous nuclei that migrate toward the iPP phase, even though the extent of such a migration phenomenon is much higher from the EPR_{Ti} phase (see also Table 5). In addition for a given iPP/EPR pair the observed shift to higher temperatures increases with increasing the EPR content, thus indicating that the number of heterogeneous nuclei for the iPP volume unit, i.e. the nucleation density of the iPP phase, is composition dependent.

A shift to higher temperatures in the blend is also undergone in the non-isothermal crystallization curve of EPR_{Ti} ethylenic sequences, the maximum being found at 110°C. Taking into account that the crystallization process of the PE sequences starts in the presence of iPP crystals it could be supposed that the observed shift is caused by a nucleating ability of the iPP solid phase for PE crystal growth. Heterogeneous nuclei, owing to their comparatively higher interfacial free energy with respect to molten iPP, could also migrate from iPP phase toward EPR_{Ti} phase. Note moreover that the range of non-isothermal crystallization temperatures shown by the iPP phase crystallizing from $(60/40)_{Ti}$ melt is found very close to that shown by the EPR_{Ti} ethylenic sequences (see Table 5) indicating that the crystallization processes of iPP and PE phase could be correlated as suggested also by the observed reduction in the crystallinity degree of the two components in the (60/40) blends (see Table 5).

3.3. Phase structure

3.3.1. Mode and state of dispersion of the minor component

The analysis by SEM of the mode and state of dispersion of the EPR copolymers shows that with increasing the EPR content the layered structure originally developed in the injection moulded samples of the 80/20 (wt/wt) iPP/EPR blends (see Fig. 7) is dramatically modified according to the schematic model reported in Fig. 8. As shown in Fig. 8 moving from the border toward the core of the samples only two layers are found:

1. A skin layer (S) where no dispersed EPR domains can be observed; to be noted that such a layer is about 1200 μm thick irrespectively of the EPR microstructure.
2. A core showing phase separation, the same thickness (about 800 μm) was measured in samples of both EPR_{V} and EPR_{Ti} containing blends. In such a layer the EPR domains are mainly irregularly shaped, even tough spherical shaped domains can also be observed. It could be supposed that the irregularly shaped EPR domains are formed following a coalescence phenomenon undergone by primary spherical shaped particles. To be remarked that in the iPP/EPR_{Ti} blends a comparatively finer dispersion of the minor component is achieved (compare Fig. 9 with Fig. 10).

Table 5
Glass transition temperatures (T_g), apparent melting temperatures (T'_m) and crystallinity indices (X_c) for plain iPP and EPR_{Ti} and iPP/EPR blends, the range of non-isothermal crystallization temperatures for plain iPP and EPR_{Ti} and iPP/EPR blends are also reported

Sample	T_g (°C)	T'_m (°C)	X_c (blend) (%)	X_c (iPP) (%)	Range of non-isothermal crystallization temperatures (°C)
iPP	16	164	41	41	121 ÷ 92
EPR_{Ti}	− 41	122*	6.0	—	111 ÷ 88
$(60/40)_{Ti}$	14, − 40	163	21	35	131 ÷ 114
	—	122	1.2	—	113 ÷ 105
$(60/40)_{V}$	14, − 43	163	24	40	125 ÷ 98

[a]Polyethylenic sequences.

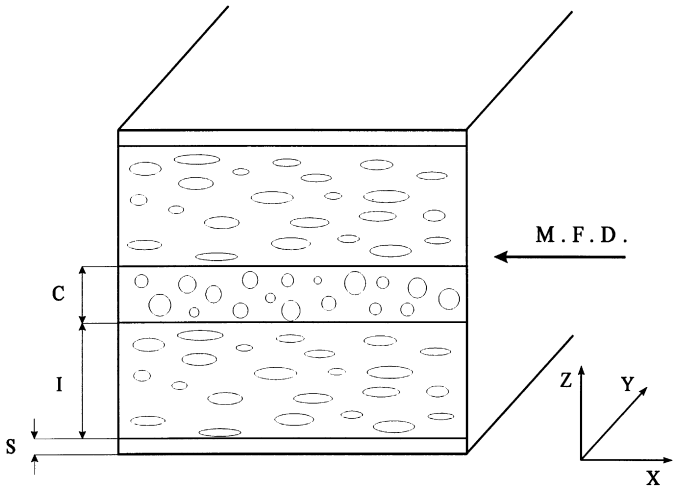

Fig. 7. Schematic model of the layered structure generated in injection moulded samples of 80/20 (wt/wt) iPP/EPR$_{Ti}$ and iPP/EPR$_{V}$ blends.

The above morphological results indicate that:

- for the 60/40 (wt/wt) iPP/EPR blend composition the EPR copolymer is the dispersed phase;
- the EPR mode of dispersion is independent of the EPR microstructure;
- the EPR dispersion coarseness increases with an increasing melt viscosity, i.e. with increasing phase viscosity ratio defined as $\mu = \eta_1/\eta_2$ where η_1 is the viscosity of the dispersed phase and η_2 that of the matrix.

The type of dependence of the size of the dispersed particles upon the phase viscosity ratio observed for all the iPP/EPR systems investigated so far agrees at least qualitatively with the prediction of the Taylor–Tomotika theory [22–24]. According to this theory plot of average particle diameter ($\bar{D}_n$) versus log μ should show a minimum in the vicinity of $\mu = 1$ (see Fig. 11). Referring to Fig. 11 the different dispersion degree shown by EPR$_{Ti}$ and EPR$_{V}$ copolymers, was accounted for by assuming that the data points of iPP/EPR blends containing such EPR phases lie on the left-hand branch of the curve, the data point of the iPP/EPR$_{Ti}$ blends tending to approach the minimum predicted by the theory.

3.3.2. Wide angle X-ray scattering analysis

The apparent crystal size (D) of the plain iPP and iPP phase crystallized in the presence of EPR copolymers in the direction perpendicular to the (110), (130) and (040) crystallographic planes was calculated by the Sherrer equation [8]:

$$D_{hkl} = \frac{K\lambda}{\beta_o \cos(\theta_{hkl})}$$

where β_o is the half width in radians of the reflection corrected for instrumental broadening, λ is the wavelength of the radiation used (1.5418 Å). The shape factor K is set equal to unity and so the size data have to be considered as relative data.

The D values calculated for plain iPP and its blends are reported in Table 6 together with the ratio between the $D_{(110)}$ values and $D_{(040)}$ values, the absence in the WAXS diffractograms of (220) reflection did not allow the correction for lattice distortion of $D_{(110)}$. The apparent crystal sizes of the iPP phase crystallized in the presence of both EPR phases are higher in direction perpendicular to the (110) crystallographic plane and lower in direction perpendicular to (040) crystallographic plane than that respectively shown by the plain iPP. The $D_{(130)}$ values in the blends being, within the experimental error, comparable to that found

Table 6
Apparent crystal size (D) of plain iPP and iPP/EPR blends together with the $D_{(110)}/D_{(040)}$ ratios

Sample	$D_{(110)}$ (Å)	$D_{(130)}$ (Å)	$D_{(040)}$ (Å)	$D_{(110)}/D_{(040)}$
iPP	94	94	149	0.63
$(60/40)_{Ti}$	99	90	78	1.27
$(60/40)_{V}$	105	91	75	1.40

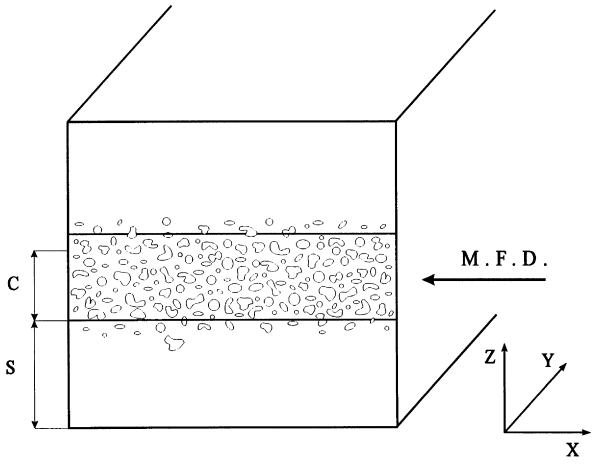

Fig. 8. Schematic model of the layered structure generated in injection moulded samples of 60/40 (wt/wt) iPP/EPR$_{Ti}$ and iPP/EPR$_{V}$ blends.

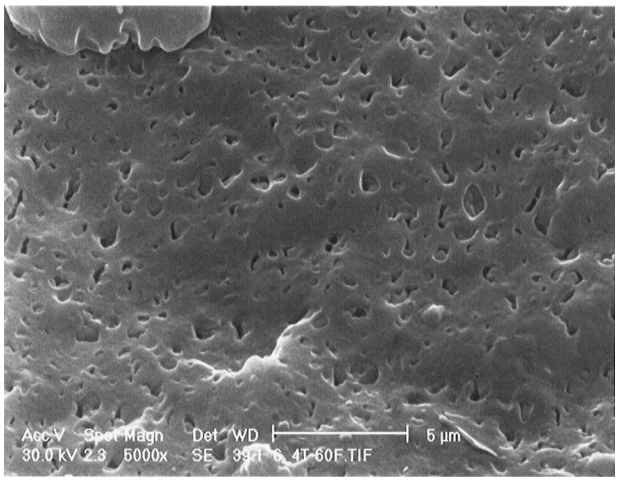

Fig. 9. SEM micrograph of surfaces of iPP/EPR$_{Ti}$ blends fractured at −60°C (5000 ×).

for the plain iPP (see Table 6). Such structural results suggest that for iPP phase crystallized in the presence of 40% of EPR phase the crystal growth in the directions perpendicular to the (110) and (040) crystallographic planes are larger and smaller than that respectively shown by the plain iPP. From the above it follows that the lamellar crystals grown in directions perpendicular to the (110) and (040) crystallographic planes of iPP phase crystallized in presence of 40% wt/wt of EPR phase have sizes whose ratio is twice as high as that shown by the plain iPP. Assuming that the folding surface of the iPP lamellar crystal is perpendicular to the *c*-axis of the iPP monoclinic unit cell, the $D_{(110)}/D_{(040)}$ ratio represents the ratio between the apparent crystal size in direction parallel to the *a**-axis (the *a**-axis being the radial growth direction of the spherulite) and the apparent crystal size in direction parallel to the *b*-axis (D_a*/D_b). Higher D_a*/D_b ratio values indicate that thicker lamellae are formed in the direction of the radial growth of the iPP spherulites in line with DSC results, i.e. with an higher number of nuclei for iPP volume units and consequently crystal growth

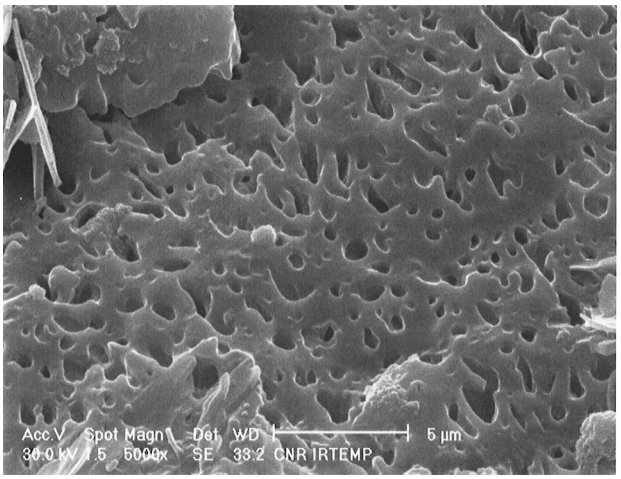

Fig. 10. SEM micrograph of surfaces of iPP/EPR$_V$ blends fractured at −60°C (5000 ×).

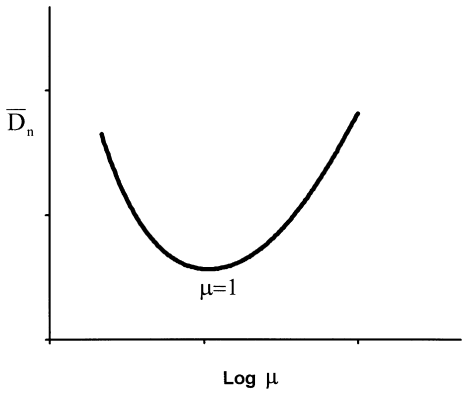

Fig. 11. Average size ($\bar{D}_n$) of dispersed particles as a function of the logarithm of phase viscosity ratio (μ), the trend as predicted by Taylor–Tomotika.

occurring at lower undercooling. For the iPP phase crystallized in the presence of a lower EPR content (20% wt/wt) the $D_{(110)}/D_{(040)}$ ratio was found, on the contrary, constant being comparable to that determined for plain iPP [6].

3.3.3. Small angle X-ray scattering analysis

Typical Lorentz corrected desmeared patterns for the iPP/EPR blends are shown in Fig. 12, note that for both the blends defined maxima are exhibited by the desmeared SAXS profiles. Therefore from the L values, calculated by applying the Bragg's law, the value the crystalline lamellar thickness (L_c) was calculated by using the following relation:

$$L_c = \frac{X_c \cdot L}{(\rho_c/\rho_a)(1 - X_c) + X_c}$$

where X_c is the crystallinity index and ρ_c and ρ_a are the densities of the crystalline and amorphous iPP phase, respectively [25]. Subtracting the obtained L_c value from the L value the average thickness of the amorphous inter-lamellar layer (L_a) was obtained. The L, L_c and L_a values so obtained are reported in Table 7 for plain iPP and its blends with EPR$_{Ti}$ and EPR$_V$ copolymers. As shown in Table 7 the L_{iPP} and $L_{iPP/EPR}$ values are to be considered within the experimental error (± 5 Å) in agreement with results obtained while studying both the same and different iPP/EPR blends [2–6]. It is interesting to observe that when iPP crystallizes from $(60/40)_{Ti}$ melt the phase structure developed in such blends is characterized by amorphous inter-lamellar layers higher than that shown by the plain iPP. Such a finding could be accounted for by hypothesizing

Table 7
Long period (L), lamellar thickness (L_c) and inter-lamellar amorphous thickness (L_a) for plain iPP and iPP/EPR blends

Sample	L (Å)	L_c (Å)	L_a (Å)
iPP	135	52	83
$(60/40)_{Ti}$	142	47	95
$(60/40)_V$	137	52	85

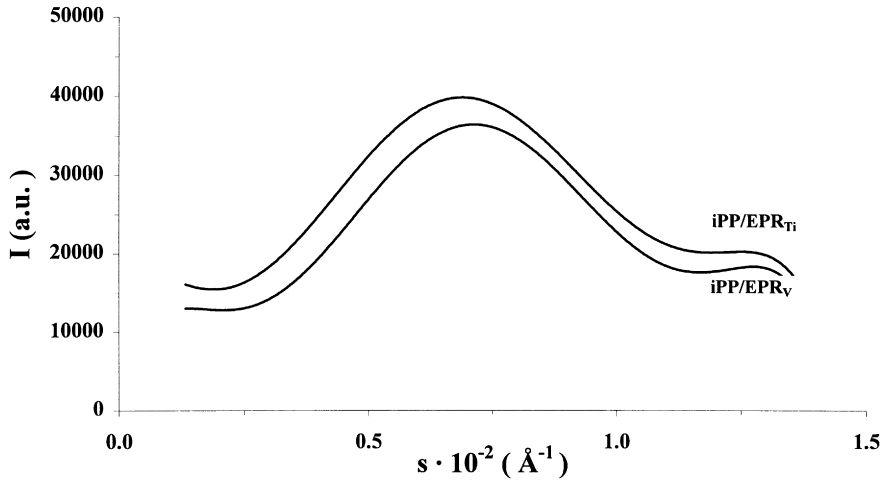

Fig. 12. Desmeared SAXS profiles for iPP/EPR blends.

that crystalline domains of EPR_{Ti} ethylenic sequences remain entrapped in the iPP amorphous interlamellar regions, thus increasing its thickness and hindering the iPP crystal growth. DSC experiments showed in fact that the 40% (wt/wt) of EPR_{Ti} copolymer strongly interferes with the crystallization process of the iPP phase and that the crystallization processes of the EPR_{Ti} ethylenic crystallizable sequences and of the iPP phase could be correlated. The observed increase in iPP L_a value could also be caused by a diffusion of EPR_{Ti} molecules with a distribution of composition and length of sequences of structural units approaching that of the plain iPP into the iPP inter-lamellar amorphous layer with formation of EPR_{Ti} amorphous domains more or less interconnected with the amorphous iPP phase. It is interesting to note that the super-reticular parameters of iPP phase crystallized in the presence of EPR_{Ti} copolymer depend on blend composition, i.e. the L_c and L_a values decrease and increase with the EPR_{Ti} content (wt/wt), respectively. Work is in progress to assess the validity of the results so far obtained comparing by SAXS the superstructure shown by the iPP phase crystallized in the presence of 70% (wt/wt) of EPR_{Ti} copolymer with that exhibited by iPP phase crystallized in the presence of 70% (wt/wt) EPR_V copolymer.

3.4. Impact behaviour

The notched Izod impact strength values of the plain iPP and iPP/EPR_{Ti} and iPP/EPR_V materials are reported in Fig. 13 as a function of the copolymer content (wt/wt) for test temperatures of -60°C and -30°C, for higher test temperatures such materials are do not broken. As shown in Fig. 13 for temperatures below the EPR T_g (-60°C) the iPP impact strength can be improved by adding the 40% of EPR copolymer (wt/wt), note that the impact strength value shown by the iPP/EPR_V material is almost twice as high as that exhibited by the iPP/EPR_{Ti} material. Such a result could be ascribed to their different state of dispersion (shape

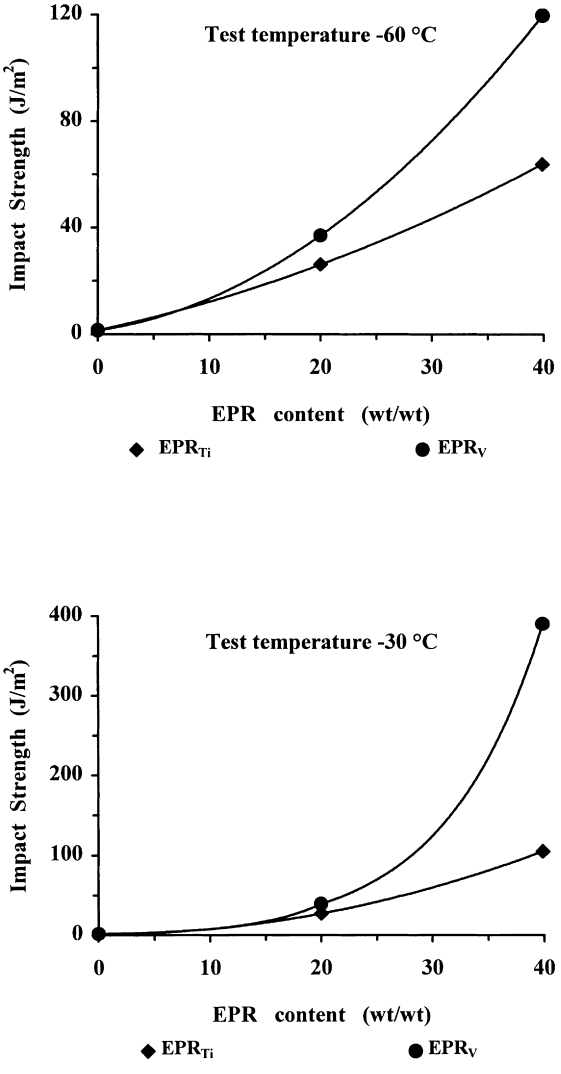

Fig. 13. Notched Izod impact strength as a function of temperature for plain iPP and iPP/EPR blends.

and size of domains and/or shape and size distribution of domains) (compare Fig. 9 and Fig. 10). It is interesting to underline, moreover, that the fracture surfaces of both the iPP/EPR_V and iPP/EPR_{Ti} blends exhibit a stress-whitening phenomenon with comparable intensity localized in the central part of the samples, where the maximum concentration of domains of dispersed phase occurs. Therefore, it could be hypothesized that in the blends containing the EPR_{Ti} phase both cavitation process and multicrazes formation are to be associated with the observed whitening, and/or the mechanism of multicrazes formation in such blends is comparatively less active in avoiding fracture.

For test temperatures closer to the EPR T_g and lower than the iPP T_g ($-$ 30°C) better properties are confirmed to be shown by the blends containing the EPRV copolymer (see Fig. 13). For such a temperature the impact strength value exhibited by the iPP/EPR_V blends results almost five times as high as that shown by the iPP/EPR_{Ti} blends. The fracture surfaces of both iPP/EPR_V and iPP/EPR_{Ti} blends broken at $-$ 30°C show a stress whitening phenomenon slightly more pronounced than that observed in samples broken at $-$60°C. The very different behaviour of EPR_{Ti} and EPR_V copolymers as impact modifiers (see Fig. 13) could be related both to their different dispersion coarseness and microstructure. The ethylenic crystallinity shown by the EPR_{Ti} phase could induce toughening deterioration by a decrease of the molecules density in the EPR_{Ti} domains, notwithstanding the beneficial effect of the ethylenic lamellar build-up [26]. Such a hypothesis seems to be supported by the comparatively higher value of the elastic modulus (680 MPa) shown by the iPP/EPR_{Ti} materials, the iPP/EPR_V materials showing a modulus value equal to 540 MPa.

4. Conclusions

A study aimed at investigating effects of EPR microstructure and content on melt rheology, phase morphology and properties of (60/40) iPP/EPR pairs was performed. The following is to be remarked:

- The iPP/EPR blends investigated in this work are to be classified as 'negative deviation blends'.
- SEM analysis performed on injection moulded samples showed that for (60/40) composition the copolymers represent the dispersed phase, the irregularly shaped EPR domains being concentrated in a layer 800 μm thick localized in the core of the bars and the dispersion coarseness of such domains increasing with increasing EPR melt viscosity.
- A considerable improvement in the iPP impact strength at low test temperatures is obtained, for a given temperature comparatively better impact properties are shown by the blends containing the EPR phase with a microstructure typical of a random copolymer.
- The EPR microstructure can affect both the crystallization process of iPP phase and the inner structure of the iPP spherulites [crystalline lamellar thickness (L_c) and amorphous interlayer thickness (L_a)].
- WAXS studies revealed that the EPR content can influence the ratio between the iPP crystal size in a direction parallel to the *a**-axis and the crystal size in a direction parallel to the *b*-axis of the iPP monoclinic unit cell.

References

[1] D'Orazio L, Mancarella C, Martuscelli E. Polymer 1991;32:1186.
[2] D'Orazio L, Mancarella C, Martuscelli E, Sticotti G. J Mater Sci 1991;26:4033.
[3] D'Orazio L, Mancarella C, Martuscelli E, Sticotti G. Polymer 1993;34:3671.
[4] D'Orazio L, Mancarella C, Martuscelli E, Sticotti G. J Appl Polym Sci 1994;53:387.
[5] D'Orazio L, Mancarella C, Martuscelli E, Sticotti G. Advanced routes for polymer toughening, chap. 5. Amsterdam: Elsevier, 1996.
[6] D'Orazio L, Mancarella C, Martuscelli E, Sticotti G. J Appl Polym Sci, in press.
[7] Vonk CG. J Appl Crystall 1975;8:340.
[8] Alexander LE. X-ray diffraction in polymer science. New York: Wiley, 1969.
[9] Lee BL, White JL. Trans Soc Rheol 1975;19:481.
[10] Utraki CA, Kamal MR. Polym Engng Sci 1982;22:96.
[11] Nielsen LE. Polymer rheology. New York: Marcel Dekker, 1977.
[12] Han CD. J Appl Polym Sci 1986;32:3809.
[13] Han CD. J Appl Polym Sci 1988;35:167.
[14] Ferry JD. Viscoelastic properties of polymers, 2nd ed. New York: Wiley, 1970.
[15] Nielsen LE. Mechanical properties of polymers and composites, vol. 1. New York: Marcel Dekker, 1974.
[16] Cox WP, Merz EH. J Polym Sci 1958;28:619.
[17] Onogi S, Masuda T, Ibaragi T. Kolloid Z 1968;222:110.
[18] Onogi S, Fujii T, Kato H, Ogihara S. J Phys Chem 1964;68:1598.
[19] Verser DW, Maxwell B. Polym Engng Sci 1970;10:122.
[20] Cross MM. J Appl Polym Sci 1969;13:765.
[21] Iwakura K, Fujimura T. J Appl Polym Sci 1975;19:1427.
[22] Van Krevelen DW. Properties of polymers. New York: Elsevier, 1976.
[23] Taylor GI. Proc R Soc Lond (A) 1934;146:501.
[24] Tomotika S. Proc R Soc Lond (A) 1934;150:322.
[25] Tomotika S. Proc R Soc Lond (A) 1936;153:322.
[26] Karger-Kocsis J. Polymer Bull 1996;36:119.